Effect of loading frequency ratio on multiaxial fatigue failure of 30CrMnSiA steel

Tianqi Liu [a, b, 1], Xinxin Qi [a, 1], Xinhong Shi [a, *], Limin Gao [b], Tian Zhang [b], Jianyu Zhang [c]

[a] School of Aeronautic Science and Engineering, Beihang University, Beijing 100191, China

[b] Beijing Key Laboratory of Civil Aircraft Structures and Composite Materials, COMAC Beijing Aircraft Technology Research Institute, Beijing 102211, China

[c] College of Aerospace Engineering, Chongqing University, Chongqing 400044, China

[*] Correspondence：shixinhong@buaa.edu.cn

[1] Tianqi Liu and Xinxin Qi contributed equally to this work and should be considered co-first authors

Abstract: Multiaxial fatigue experiments under asynchronous loadings with four different loading frequency ratios were carried out on 30CrMnSiA steel. The experimental results show that the fatigue life decreases when the axial or torsion frequency increases from 1 to 2, while there is no significant change when the axial or torsion frequency increases from 2 to 4. The surface crack paths are observed and show that cracks initiate on the maximum shear stress amplitude planes, propagate approximately tens of microns, and then turn to propagate along the maximum normal stress planes. The number of secondary cracks increases when the axial or torsion frequency increases. Subsequently, the Bannantine-Socie and Wang-Brown cycle counting methods along with various multiaxial fatigue criteria and Palmgren-Miner's cumulative damage rule were used for fatigue life prediction. The experimental results are consistent with the fatigue life predicted by the Bannantine-Socie method with the section critical plane criterion for 30CrMnSiA steel under asynchronous loading paths.

Keywords: 30CrMnSiA steel; crack growth path; fatigue life prediction; asynchronous loading; frequency ratio

1. Introduction

In engineering practice, the multiaxial fatigue failure behavior of structures and components is affected by the phase angle, mean stress, loading sequence, stress/strain amplitude ratio and different frequency ratios of tensile and shear stress/strain components (asynchronous loadings). Compared with other multiaxial loading paths, there are limited number of studies on multiaxial asynchronous loadings.

In most studies[1-3], the asynchronous loading path is usually considered as one type of multiaxial loading path. The commonly used frequency ratios[4-6] of tensile to shear stress or strain are 2:1 and 1:2. Mielke[7] conducted asynchronous loading tests on 25CrMo4 steel and concluded that the fatigue limit decreases when the tensile or shear frequency ratios increase. Similar conclusions were drawn by McDiarmid[8-10] for EN24T steel, by Heidenreich et al.[11] for 34Cr4 steel, and by Bernasconi et

al.[12] for 39NiCrMo3 steel. Experiments using 42CrMo4 steel were carried out by Reis et al.[13], and the frequency ratios were 2:1 and 1:2 with a constant stress amplitude ratio of $1/\sqrt{3}$. By using the shear-based models, the experimental results of crack initiation are consistent with the estimated direction. In order to study the effect of asynchronous load on the stress-strain response of materials, four steel and aluminum alloy materials under nine different strain asynchronous loading paths were tested by Pejkowski and Skibicki[14]. The results show that asynchronous loading paths cause nonproportional hardening, and they have a significant effect on fatigue failure life. The definition of fatigue cycles was discussed under an asynchronous loading path. Pejkowski and Seyda[15] observed the small cracks in four materials under asynchronous loadings and found that cracks initiate on the maximum shear strain planes and change direction to the maximum normal strain planes.

In addition, when dealing with asynchronous loading problems, the multiaxial cycle counting method should be used. The rainflow cycle counting method[16] is the most well-known method, and reliable results can be obtained under uniaxial loading. However, its applicability is limited under asynchronous loading. The commonly used method is to treat the asynchronous loading path as a loading block[17], and the fatigue life is defined as the number of loading block repetitions. To overcome this problem, two cycle counting methods were proposed, and they are Bannantine-Socie (BS) method[18, 19] and Wang-Brown (WB) method[20-22]. The BS method[18, 19] is based on the uniaxial rainflow cycle counting method and critical plane criterion. In this method, a tensile or shear damage parameter on the critical plane is chosen, and then the number of loading reversals is accounted for. However, only the tensile or shear stress/strain is considered, and the interaction between the two parameters is ignored. The WB method[20-22] is based on the rainflow cycle counting method and the von Mises equivalent stress or strain. In this method, the effect of the loading history on fatigue damage accumulation may be ignored. Meggiolaro and de Castro[23, 24] modified the WB method and expanded the stresses or strains into the five-dimensional Euclidean space. To overcome the drawback of the WB model, Wei and Dong[25-27] proposed the concept of path dependent effective stress, and the maximum range of path dependent effective stress was selected as the first reversal cycle count. In the Shang and Wang method[28], the shear stress or strain was counted by the rainflow cycle counting method on the critical plane. Anes and coauthors[29, 30] proposed a virtual cycle counting method that is a nonrainflow cycle counting method, and it is based on the stress scale factor[31]. The model was validated for 42CrMo4, 1050QT and 304L steel under 11 types of asynchronous strain loading paths. Lee et al.[32] performed

multiaxial fatigue tests on four steel materials using five types of triangular waveforms under asynchronous loading paths. The rainflow cycle counting method was carried out on normal and shear strain loading paths, respectively, to accumulate fatigue damage. The fatigue cycles depend on which individual strain produces more damage. Janssens[33] proposed a universal cycle counting method independent of the damage criterion, but it was not verified by experimental data. Multiaxial fatigue tests were performed by Arora et.al[34] under asynchronous loading of four different frequency ratios, and the prediction results by BS and Smith-Watson-Topper (SWT)[35] criteria are nonconservative compared with the experimental fatigue life.

In view of the above, the experimental studies have been mainly focused on fatigue limits and the direction of crack initiation under strain controlled asynchronous loading paths. The effect of frequency ratios on fatigue life and surface crack growth paths are still needs further research. In the present study, multiaxial fatigue experiments under asynchronous loading paths were performed to investigate the effect of frequency ratios on fatigue life of 30CrMnSiA steel. The surface crack growth paths were observed to determine the fatigue damage mechanism. The surface crack lengths *versus* loading blocks under asynchronous loadings were compared and analyzed. Finally, the fatigue life was predicted by a few commonly used cycle counting models and fatigue failure criteria with Palmgren-Miner's cumulative damage rule.

2. Experiments

2.1. Experimental Specimens

30CrMnSiA steel was the experimental material. Its chemical composition, weight percent and mechanical properties were given in the authors' previous study[36]. The geometry and dimensions of solid cylindrical bar specimens are shown in Figure 1.

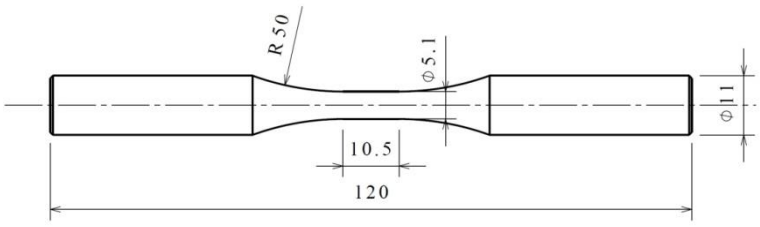

Figure 1. Shape and dimensions of specimens (unit: mm)

2.2. Experimental Procedure

The multiaxial fatigue tests were conducted on an MTS 858 testing system at room temperature and atmosphere. The loading frequency of a loading block used in the test was 0.5 Hz.

The tension-torsion stress components of multiaxial asynchronous fatigue loading are as follows

$$\sigma_x(t) = \sigma_{x,a} \sin(\xi_1 \omega t) \tag{1}$$

$$\tau_{xy}(t) = \tau_{xy,a} \sin(\xi_2 \omega t) \tag{2}$$

where the loading frequency is controlled by ξ_1 and ξ_2. In the tests, $\sigma_{x,a} = \tau_{xy,a} = 350$ MPa, and the stress amplitude ratio was 1.0 without a phase angle. The tests were conducted under four different frequency ratios (ξ_1: ξ_2) including: 2:1, 4:1, 1:2 and 1:4. The multiaxial asynchronous fatigue loading paths in a loading block with different frequency ratios are shown in Figure 2.

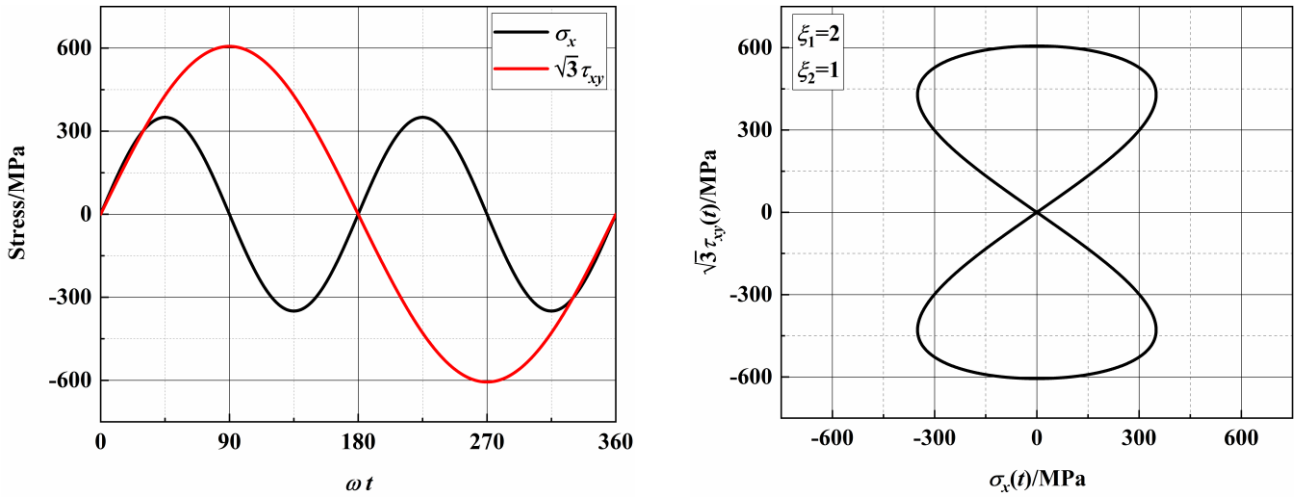

(a) ξ_1: ξ_2 = 2:1

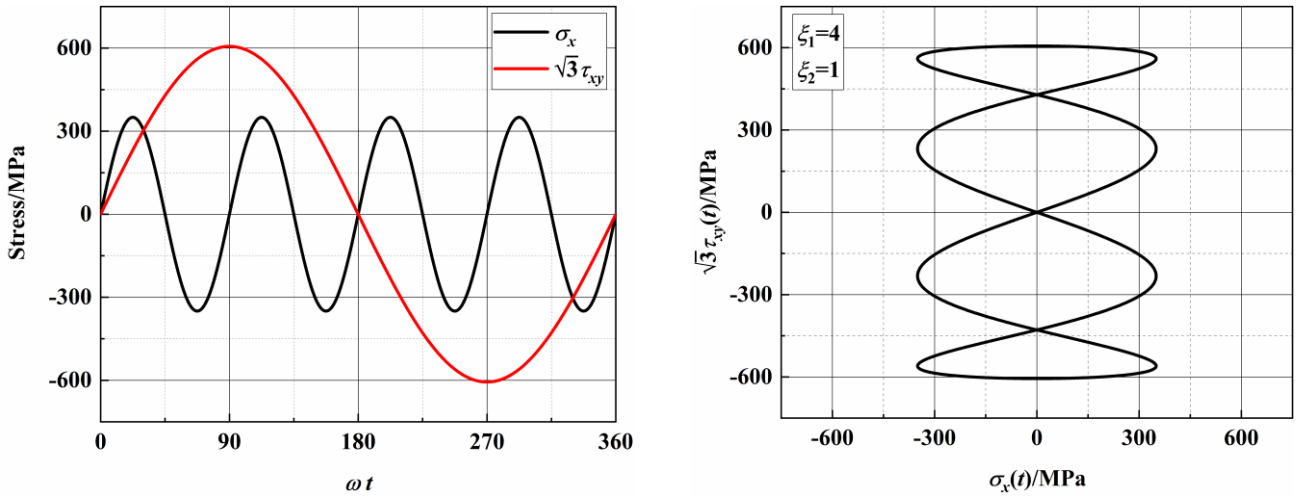

(b) ξ_1: ξ_2 = 4:1

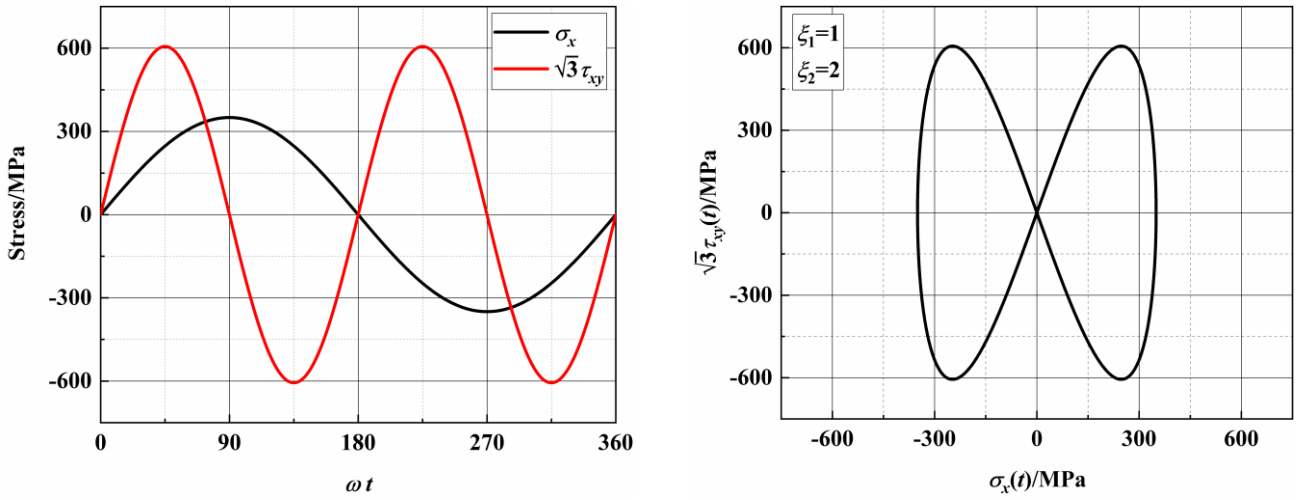

(c) ξ_1: ξ_2 =1:2

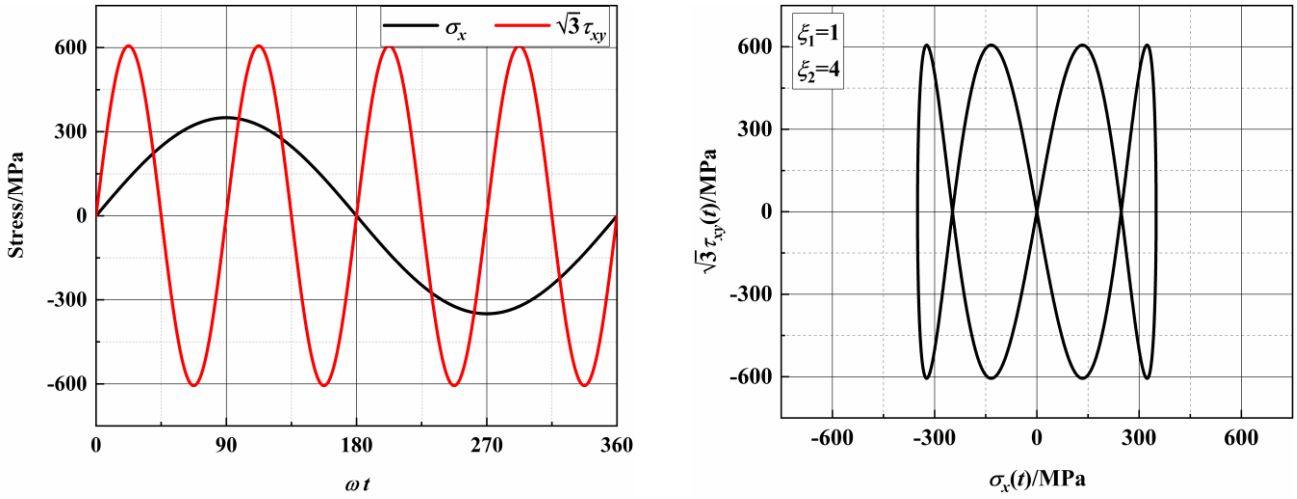

(d) ξ_1: ξ_2 = 1:4

Figure 2. Multiaxial asynchronous loading paths with different frequency ratios

3. Analysis of Experimental Results

3.1. Multiaxial Fatigue Life

Under multiaxial asynchronous loadings, the fatigue life is defined as the number of loading blocks. The logarithmic mean fatigue life is expressed as:

$$N_{50} = 10^{\left(\sum_{i=1}^{n} \log N_f\right)/n} \tag{3}$$

The experimental fatigue lives under different asynchronous loadings are listed in Table 1. The effect of frequency ratios on the multiaxial fatigue life is given in Figure 3. For $\xi_1 = \xi_2 = 1$, the experimental results can be found in the authors' previous study[36]. The fatigue life decreases when ξ_1 or ξ_2 increases. For the condition of $\xi_2 = 1$, fatigue life decreases significantly when ξ_1 increases from 1 to 2, while it decreases by 25% when ξ_1 increases from 2 to 4. For the condition of $\xi_1 = 1$, fatigue life also decreases significantly when ξ_2 increases from 1 to 2, while fatigue life has no obvious change with the increase of ξ_2 from 2 to 4.

Table 1. Test results under different frequency ratios

Load path	$\sigma_{x,a}$/MPa	$\tau_{xy,a}$/MPa	ξ_1	ξ_2	Spec. ID	N_f/blocks	N_{50}/blocks
--	350	350	1	1	G-10	185,261	141,984
					G-11	175,013	
					G-12	119,687	
					G-100	136,694	
					G-104	108,778	
AS-1	350	350	2	1	DF-4	52,632	47,560
					DF-6	42,976	
AS-2	350	350	4	1	DF-9	35,702	35,710
					DF-10	35,717	
AS-3	350	350	1	2	DF-2	49,892	50,195
					DF-5	50,500	
AS-4	350	350	1	4	DF-7	70,330	50,033
					DF-8	35,593	

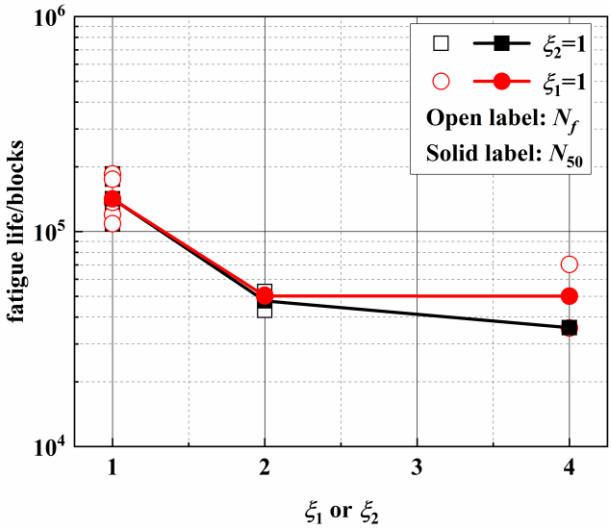

Figure 3. Frequency ratios effect on multiaxial fatigue life

3.2. Stress Analysis of Individual Loading Blocks

Under multiaxial asynchronous loading, Figure 4 shows the stress components on an arbitrary plane, and the plane orientation is defined as φ.

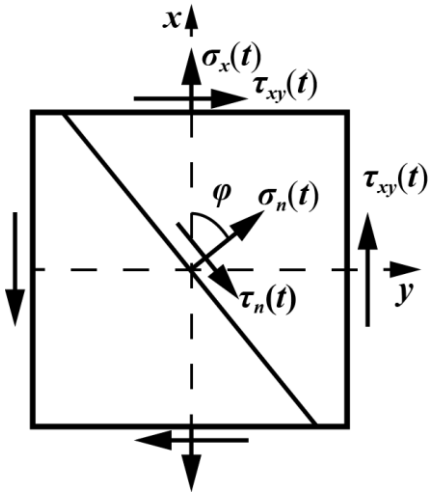

Figure 4. Stress state and plane direction under multiaxial fatigue loading

Under different frequency ratios, the stress components on a plane are calculated as

$$\sigma_n(t)=\sigma_{x,a}\cos^2\varphi\sin(\xi_1\omega t)+\tau_{xy,a}\sin 2\varphi\sin(\xi_2\omega t) \tag{4}$$

$$\tau_n(t)=-\frac{\sigma_{x,a}}{2}\sin 2\varphi\sin(\xi_1\omega t)+\tau_{xy,a}\cos 2\varphi\sin(\xi_2\omega t) \tag{5}$$

Under different frequency ratios, Table 2 shows the directions of the MSSA and MN planes, and the stresses on the two planes. In addition, the MN and MSSA on an arbitrary plane in a loading block are analyzed and given in Figure 5. There are four MSSA planes and two MN planes exist for each of the four frequency ratios in a loading block. In addition, it should be noted that there are two MSSA planes for AS-1. Two MN planes are axisymmetric about the axis of the specimen, and the values of $\tau_{n,a}$ on the two MN planes are equal.

Table 2. MSSA and MN plane orientations under different frequency ratios

Load path	ξ_1	ξ_2	MSSA	σ_n/MPa	$\tau_{na,\max}$/MPa	MN	$\sigma_{n,\max}$/MPa	$\tau_{n,a}$/MPa
AS-1	2	1	0°/90°	350/0	350.00	±30.0°	494.98	285.77
AS-2	4	1	±13.3°/±76.7°	476.59/167.43	372.16	±31.0°	544.26	307.08
AS-3	1	2	±10.0°/±80.0°	299.42/127.23	371.88	±34.0°	504.46	256.13
AS-4	1	4	±12.4°/±77.6°	385.62/161.73	385.62	±32.5°	548.07	295.18

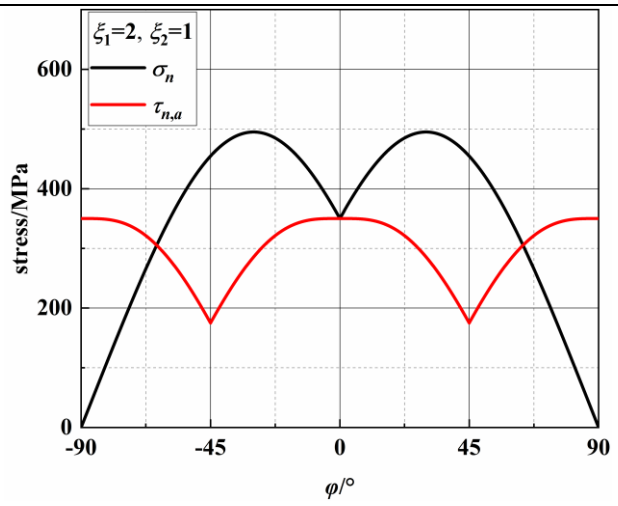

(a) AS-1

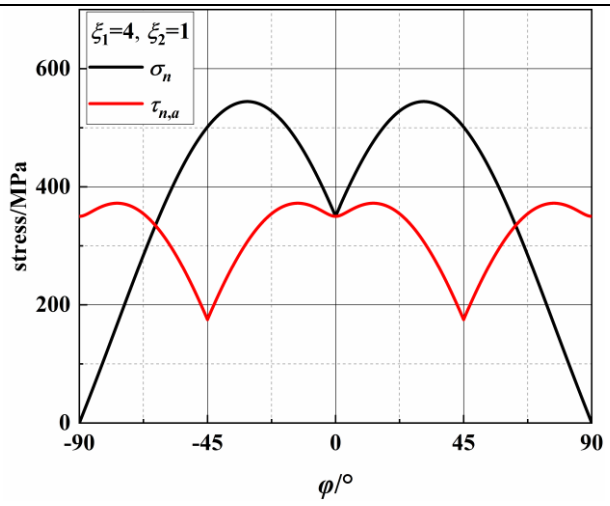

(b) AS-2

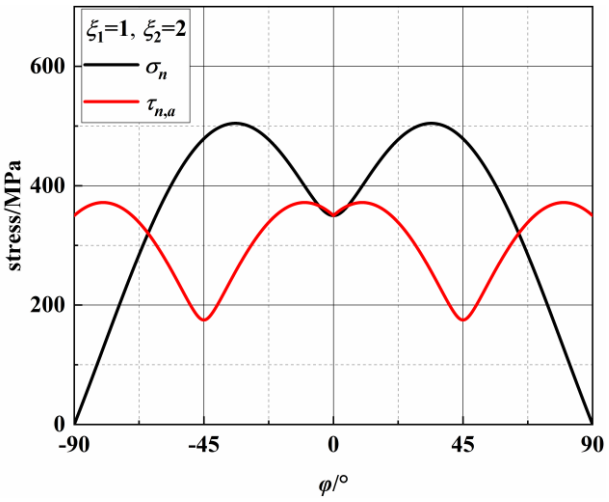

(c) AS-3

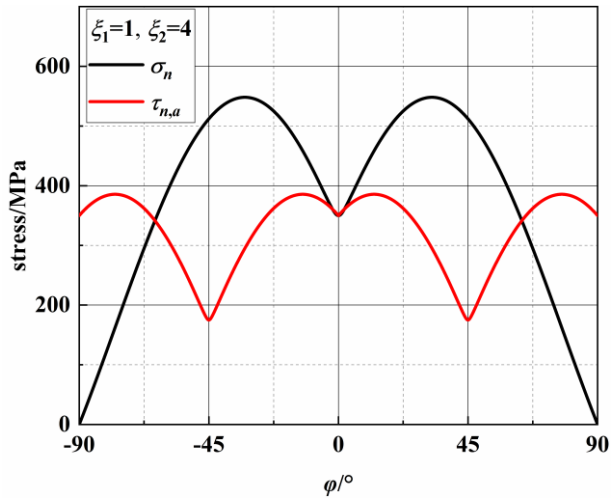

(d) AS-4

Figure 5. Variation in the stress components on different planes

According to previous research[36], the crack growth behavior is related to the stresses on the MSSA and MN planes. Figure 6 shows the stresses on the MSSA planes under four loading paths. In Figure 6(a) and (b), there are two MSSA planes, which are perpendicular and parallel to the direction of the specimen axis, respectively, when $\xi_1 = 2$ and $\xi_2 = 1$. There is only one shear stress cycle on each MSSA plane in a loading block. For normal stress, there is two cycles on the 0° plane, and the value of σ_n is zero on the 90° plane. Under AS-2 with $\xi_1 = 4$ and $\xi_2 = 1$, the directions of the MSSA planes are ± 13.3° and ± 76.7°. Each MSSA plane contains three shear stress cycles in a loading block. There are four normal stress cycles on the planes of ± 13.3°, and only one normal stress cycle with small stress on the planes of ± 76.7° as shown in Figure 6(c) – (f). When $\xi_1 = 1$ and $\xi_2 = 2$, there are two shear stress cycles on each plane in a loading block. However, it contains one larger normal stress cycle on the plane of ± 10.0° and two smaller normal stress cycles on the plane of ± 80.0° as shown in Figure 6(g) – (j). For the condition of $\xi_1 = 1$ and $\xi_2 = 4$, each of the four MSSA planes contains four normal and shear stress cycles, respectively, in a loading block. The values of MN on the plane of ± 12.4° are larger than those on the plane of ± 77.6° as shown in Figure 6(k) – (n)

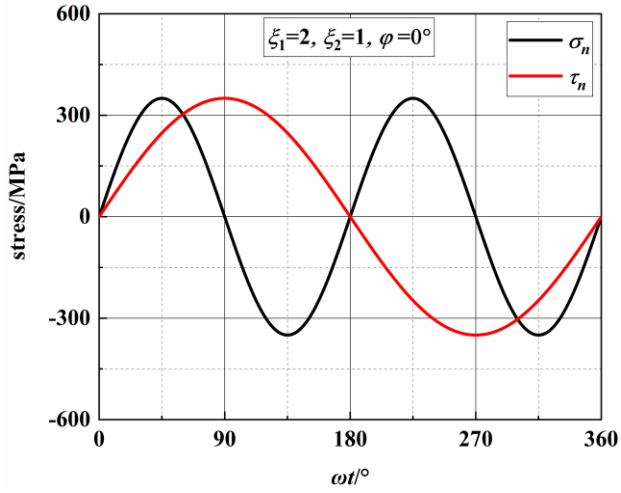

(a) AS-1, φ=0°

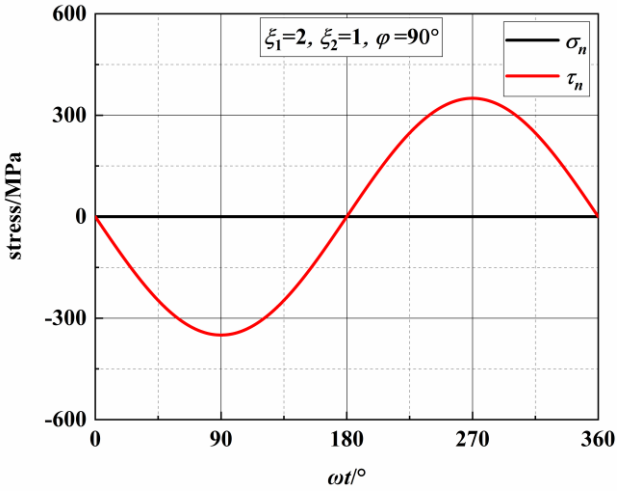

(b) AS-1, φ=90°

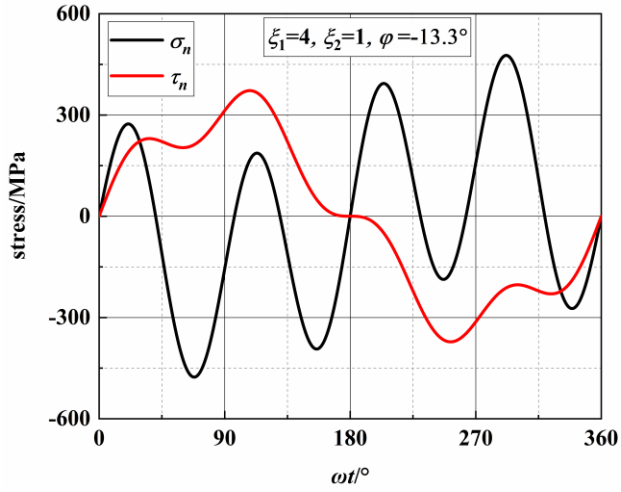

(c) AS-2, φ=-13.3°

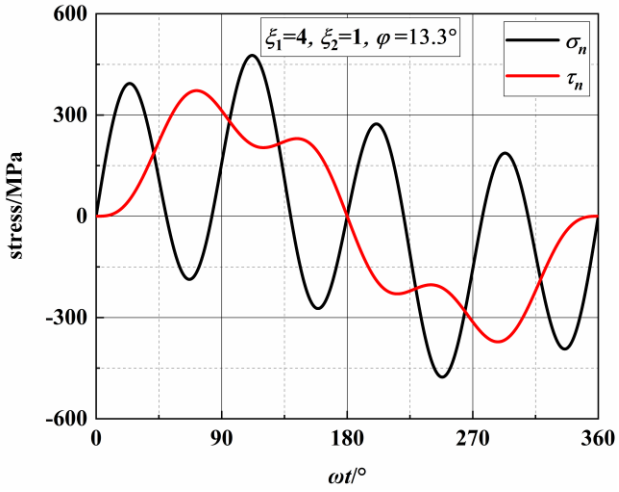

(d) AS-2, φ=13.3°

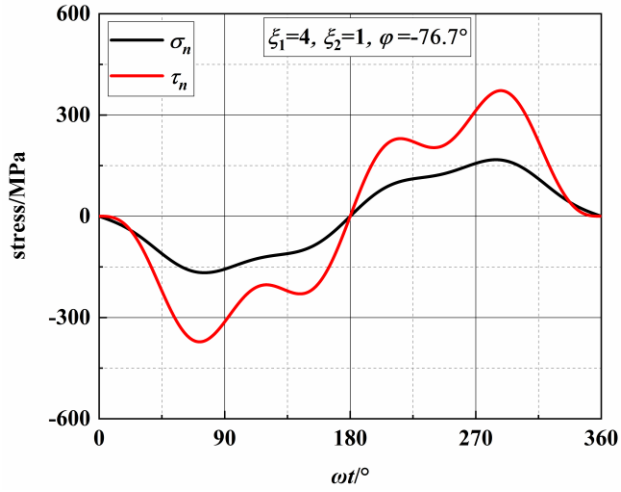

(e) AS-2, φ=-76.7°

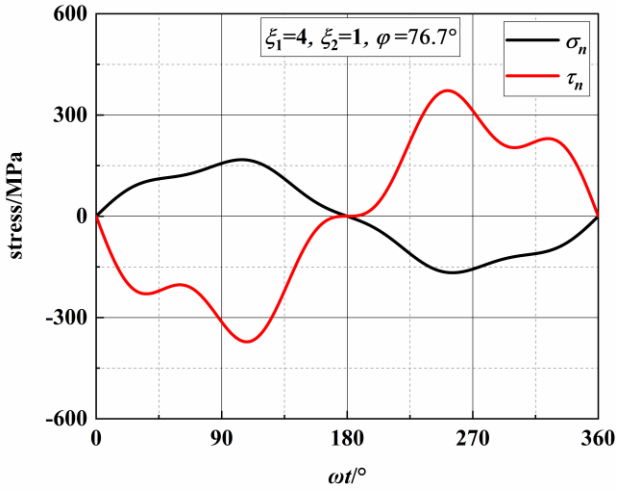

(f) AS-2, φ=76.7°

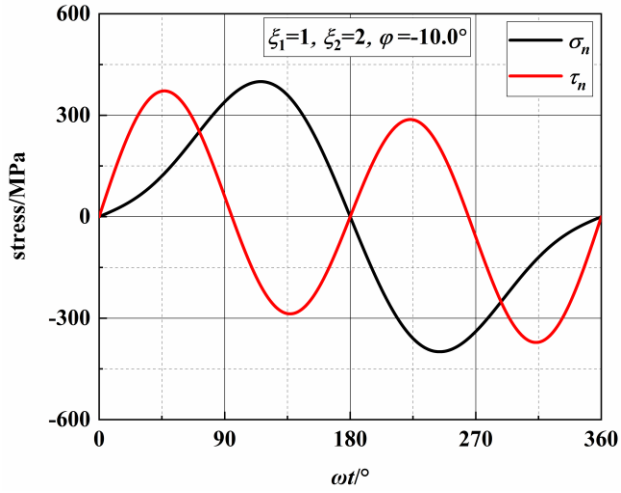

(g) AS-3, φ=-10.0°

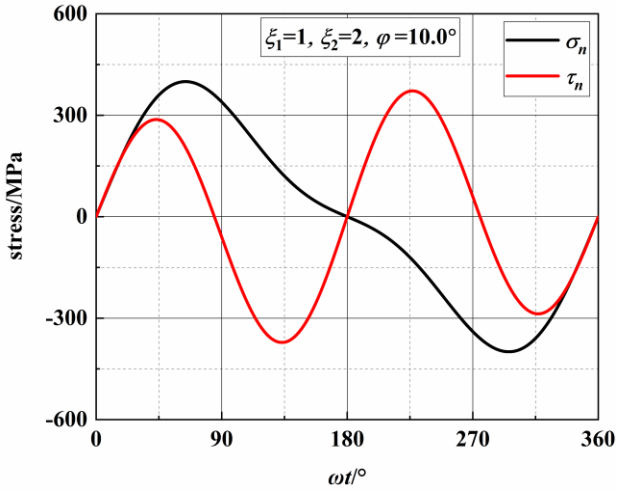

(h) AS-3, φ=10.0°

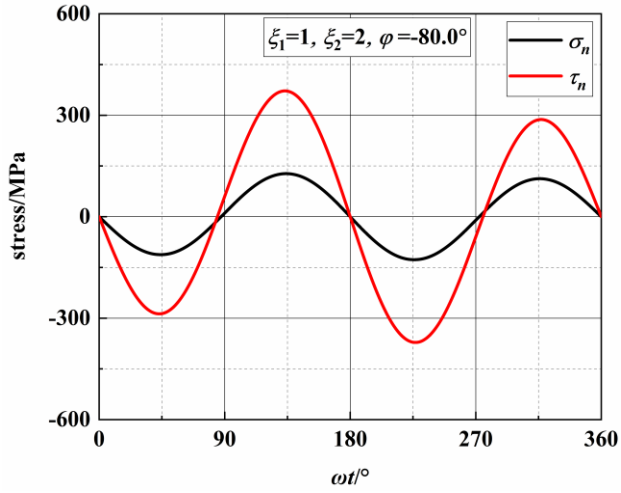

(i) AS-3, φ=-80.0°

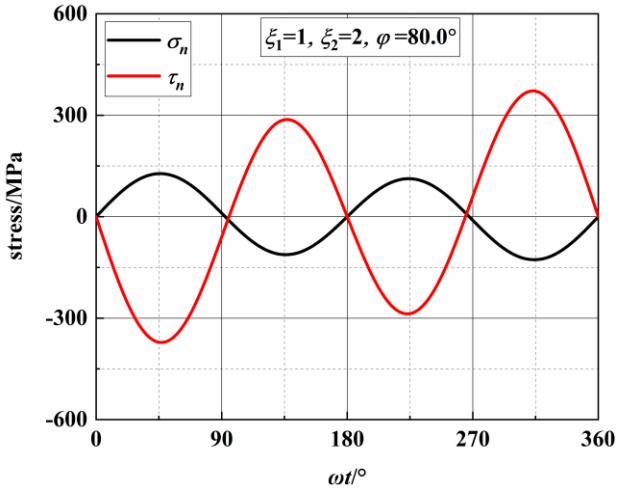

(j) AS-3, φ=80.0°

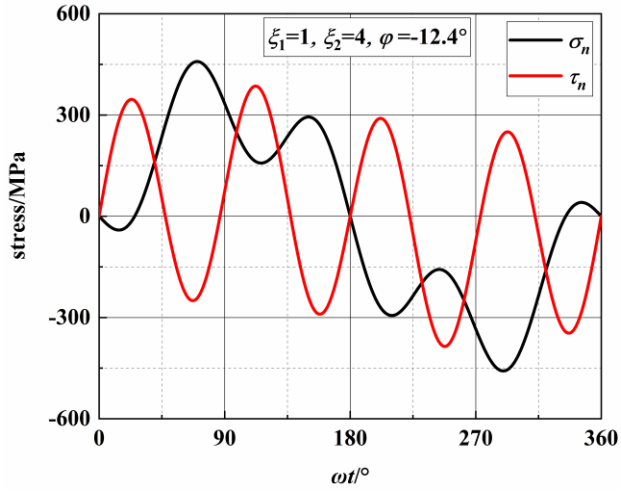

(k) AS-4, φ=-12.4°

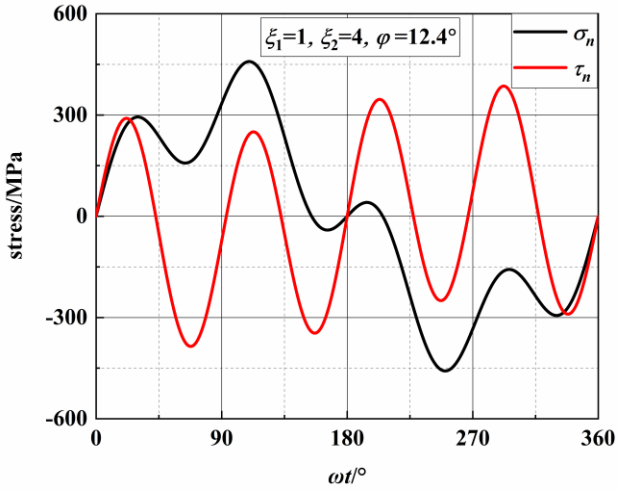

(l) AS-4, φ=12.4°

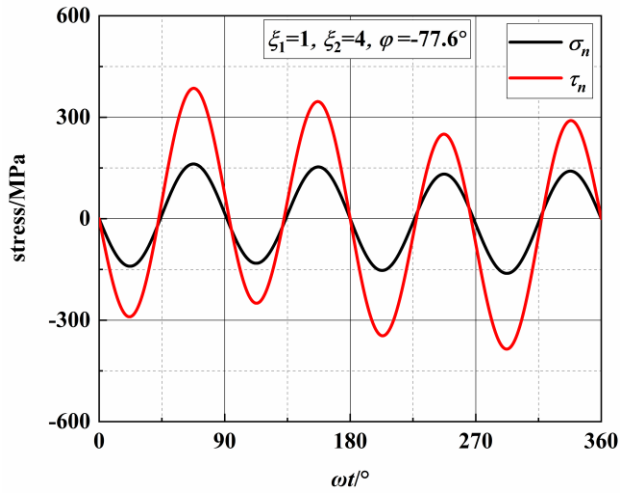

(m) AS-4, φ=-77.6°

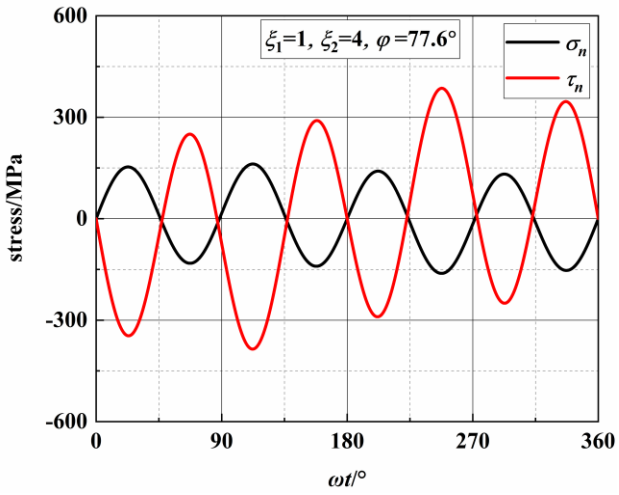

(n) AS-4, φ=77.6°

Figure 6. Variation in stresses on the MSSA plane

Under the four loading paths, the stresses on the MN planes are calculated and given in Figure 7. There are two normal and shear stress cycles on each MN plane in a loading block for the conditions of AS-1 and AS-3 and four normal and shear stress cycles for the conditions of AS-2 and AS-4.

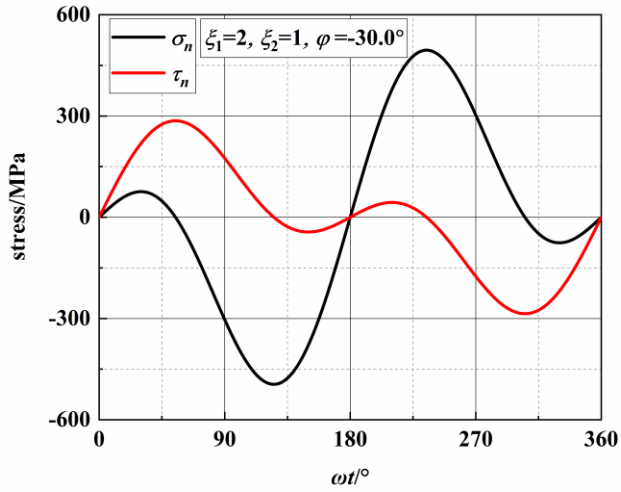

(a) AS-1, φ=-30.0°

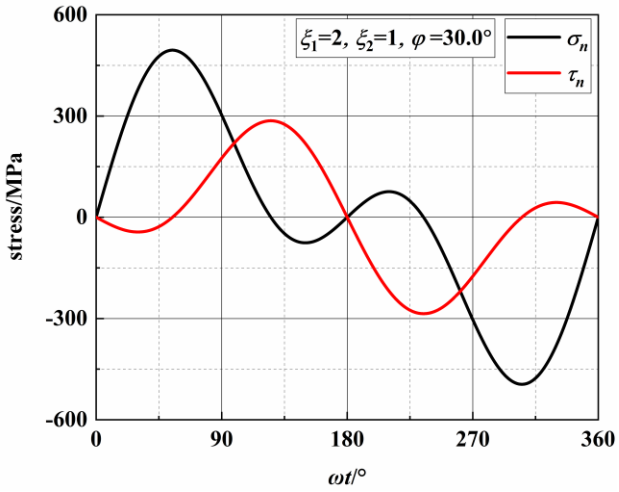

(b) AS-1, φ=30.0°

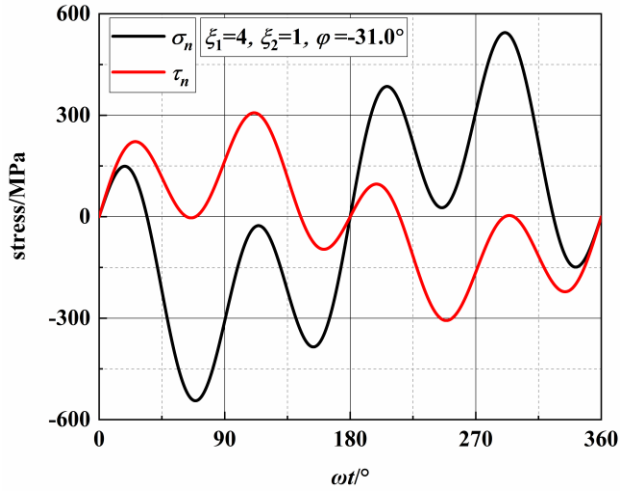

(c) AS-2, φ=-31.0°

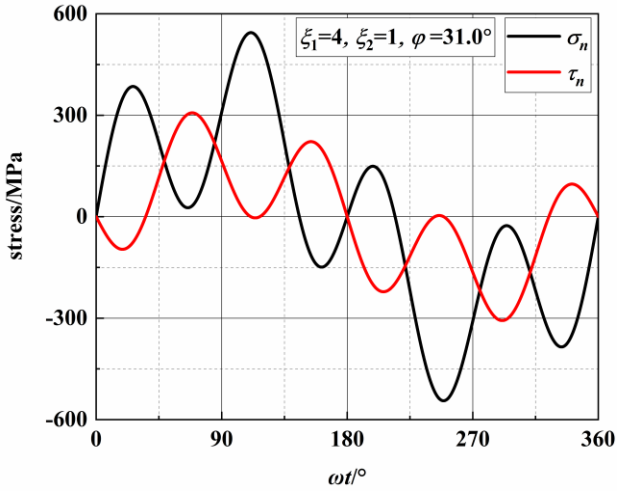

(d) AS-2, φ=31.0°

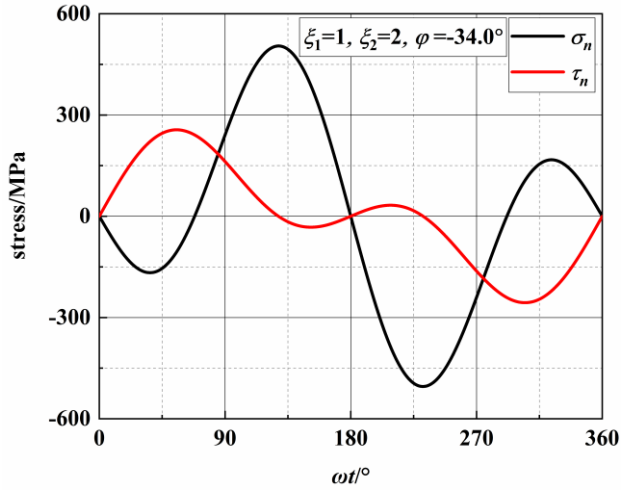

(e) AS-3, φ=-34.0°

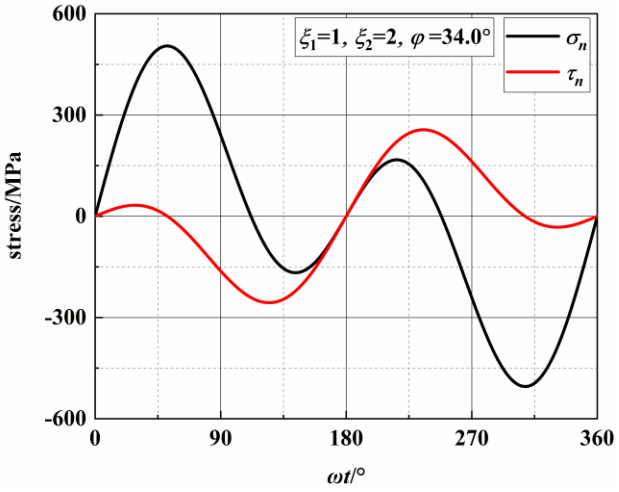

(f) AS-3, φ=34.0°

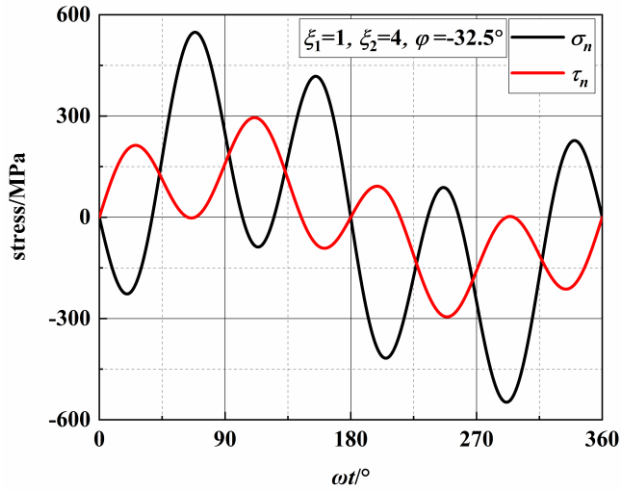

(g) AS-4, φ=-32.5°

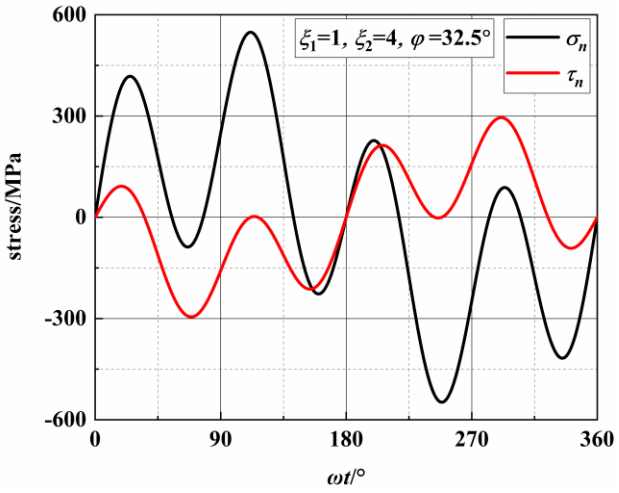

(h) AS-4, φ=32.5°

Figure 7. Variation in stresses on the MN plane

3.3. Crack Initiation and Propagation

3.3.1. Crack Growth Paths of AS-1

For the condition of $\xi_1 = 2$ and $\xi_2 = 1$, the crack morphologies of specimens DF-4 and DF-6 were observed and are shown in Figure 8. The main surface cracks of the two specimens initiate on the edge of defects; both the defects are spherical, and the diameters are approximately 34 μm for DF-4 and 21 μm for DF-6. The crack growth lengths of DF-4 on the left and right sides of the defect are approximately 30 and 55 μm at 35,000 blocks (66.5% of N_f). The crack propagation direction is close to the MN planes on the right side of the defect, while it is close to the MSSA plane, and several small cracks branch into the direction of MN planes on the left side. For specimen DF-6, Figure 8(b) shows that there are four initiation cracks along the MN planes at 35,000 blocks (81.4% of N_f). In addition, a secondary crack in DF-6 was also observed. The stage I crack and stage II cracks were both observed. The crack initiates on the MSSA plane and propagates about 10 μm, and then the cracks turn to the direction of the MN planes. The main crack propagation morphologies of specimens DF-4 at 49,500 blocks (94.0% of N_f) and DF-6 at 40,100 blocks (93.3% of N_f) are shown in Figure 8(d) and (e), respectively. The crack morphologies of DF-4 and DF-6 are similar, and the cracks propagate along the MN planes. Furthermore, the cracks branch along the MN planes of both DF-4 and DF-6 on the left and right sides of the defects as the main cracks propagate.

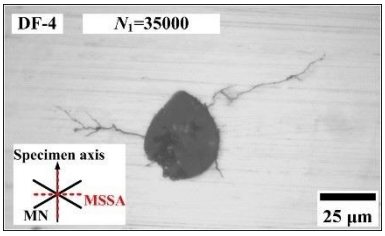

(a) Crack initiation in DF-4

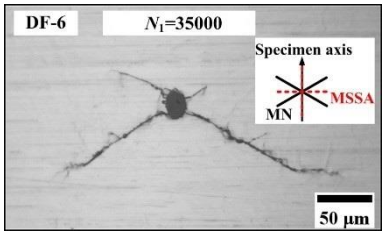

(b) Main crack initiation in DF-6

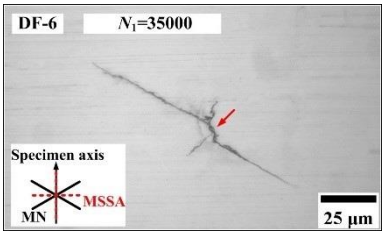

(c) Secondary crack in DF-6

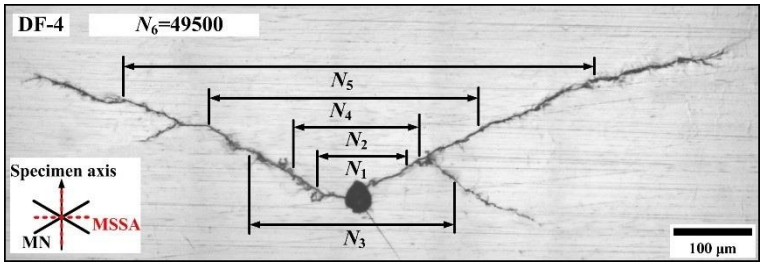

(d) Crack propagation in DF-4 (N_2 = 40,000, N_3 = 43,000, N_4 = 46,000, N_5 = 48,500)

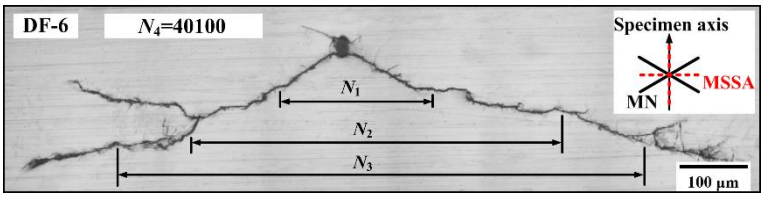

(e) Crack propagation in DF-6 (N_2 = 38,000, N_3 = 39,300)

Figure 8. Crack morphologies in specimens DF-4 and DF-6

3.3.2 Crack Growth Paths of AS-2

For the condition of $\xi_1 = 4$ and $\xi_2 = 1$, at 32,000 blocks (89.6% of N_f), six secondary cracks in specimen DF-9 were observed and the morphologies are shown in Figure 9(a) – (f). For these secondary cracks, the initiation directions are all close to the MSSA planes, which are ± 13.3° and bear larger normal stresses. However, no initiation cracks were observed on the MSSA planes of ± 76.7°. The lengths of stage I cracks are approximately 40 – 50 μm, and then the cracks propagate along the MN planes. As shown in Figure 9(g), stage I crack with length of 65 μm is observed for DF-9, and then the crack turns in the direction and branches along the two MN planes. After that, the direction of crack propagation changes again and proceeds along the direction perpendicular to the specimen axis.

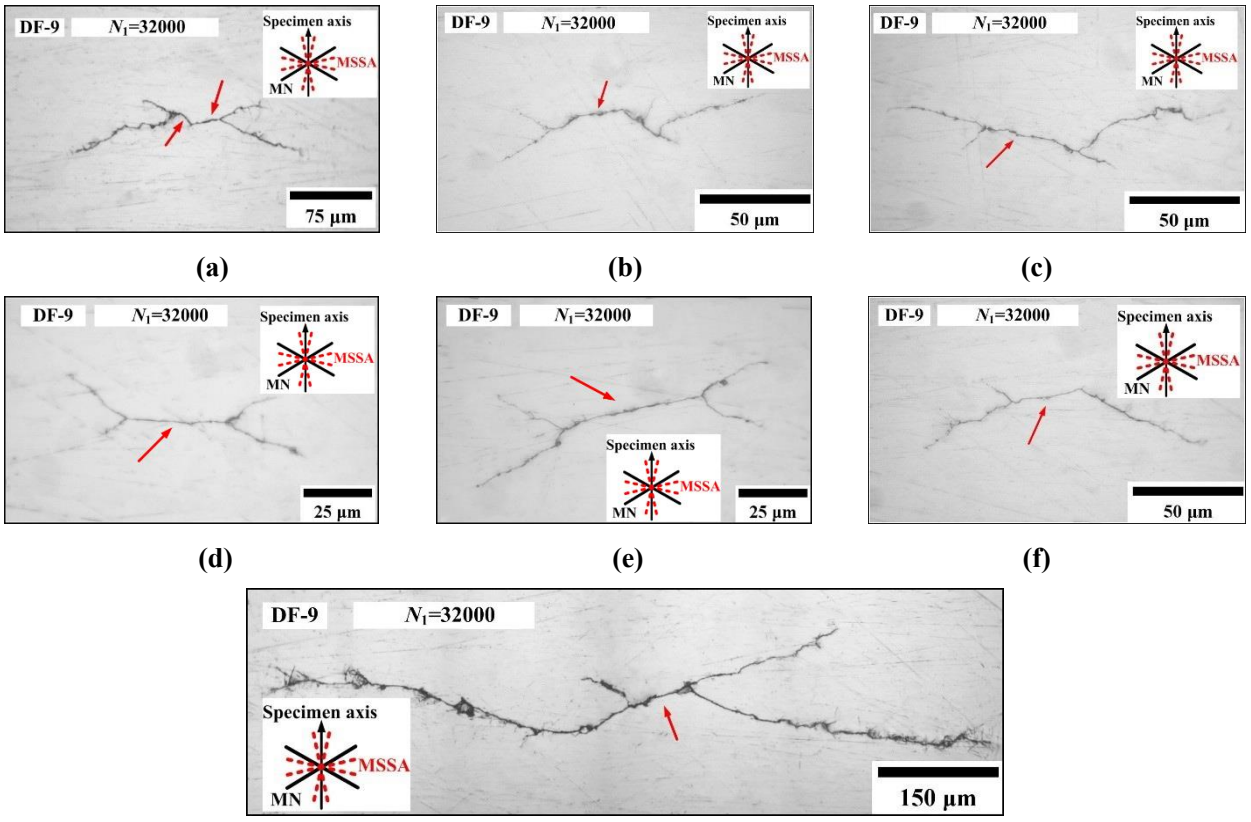

(a) **(b)** **(c)**

(d) **(e)** **(f)**

(g)

Figure 9. Secondary cracks(a), (b), (c), (d), (e) and main crack (g) in specimen DF-9

3.3.3. Crack Growth Paths of AS-3

For the condition of $\xi_1 = 1$ and $\xi_2 = 2$, Figure 10 shows the crack morphologies of DF-2 and DF-5. For DF-2 at 25,000 blocks (50.1% of N_f), the surface crack initiates on the MSSA planes and propagates along the MN planes; however, the length of the stage I crack is short which is only approximately 10 μm. For DF-5 at 25,000 blocks (49.5% of N_f), the main crack initiates on the edge of the defect and propagates along the MN planes. Otherwise, one secondary crack with a length of 150 μm was also observed at 45,500 blocks (90.1% of N_f). The transformation from stage I to stage II crack is observed. A secondary crack of DF-5 initiates on the MSSA plane with a length of approximately 35 μm and propagates along the MN planes. Figure 10(d) and (e) show the main crack propagation morphologies of specimens DF-2 at 46,000 blocks (92.2% of N_f) and DF-5 at 45,500 blocks (90.1% of N_f), respectively, and they propagate along the MN planes. For DF-5, the defect had little effect on the fatigue life. In the study[37],the critical defects for 0.13% C steels and 0.46% C steels were concluded to be 40 – 50 μm.

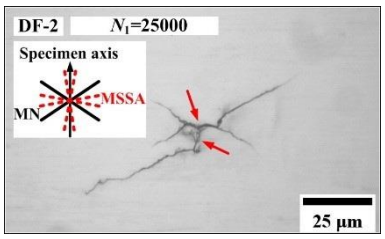

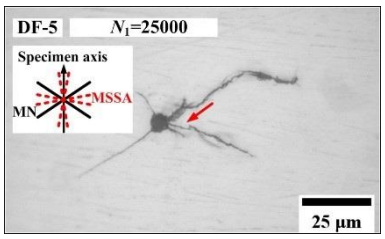

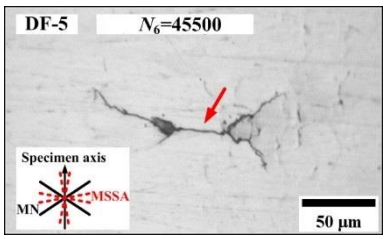

(a) Main crack initiation in DF-2 (b) Main crack initiation in DF-5 (c) Secondary crack initiation in DF-5

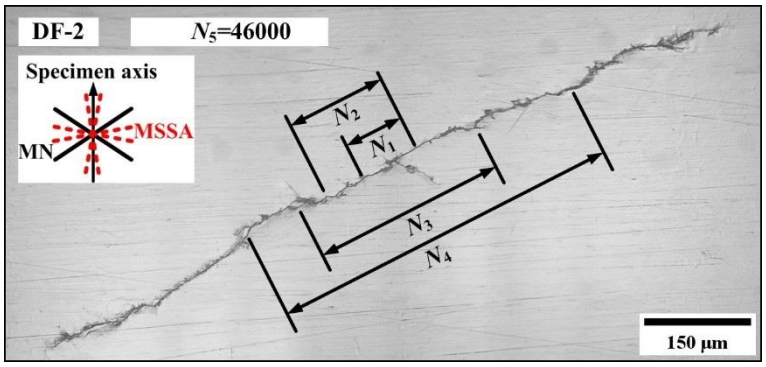

(d) Crack propagation in DF-2 (N_2 = 35,000, N_3 = 40,000, N_4 = 44,000)

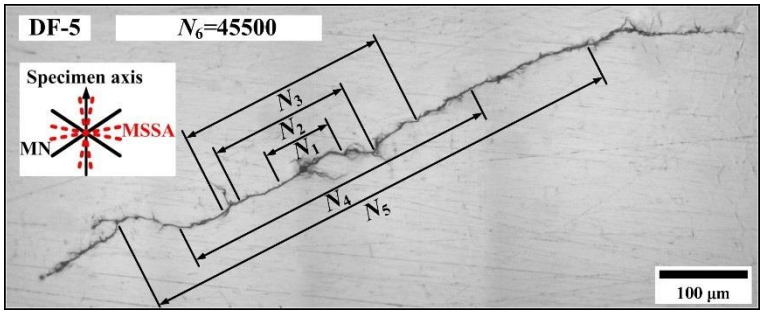

(e) Crack propagation in DF-5 (N_2 = 35,000, N_3 = 39,000, N_4 = 42,000, N_5 = 44,000)

Figure 10. Crack morphologies in specimens DF-2 and DF-5

3.3.4. Crack Growth Paths of AS-4

For the condition of $\xi_1 = 1$ and $\xi_2 = 4$, the crack morphologies of DF-7 and DF-8 are shown in Figure 11. For specimen DF-7 at 37,000 blocks (52.6% of N_f), only a stage I crack was observed and initiates along the MSSA plane. For specimen DF-8 at 20,000 blocks (56.2% of N_f), crack initiation along the MSSA plane with a length of 35 μm and propagation along the MN planes were both observed. Figure 11(c) and (d) show the main crack propagation morphologies of specimens DF-7 and DF-8, respectively. The cracks in specimens DF-7 and DF-8 propagate along the MN planes of 32.5° and-32.5°, respectively. For the specimen DF-7, the crack gradually changes direction at 5,000 blocks (71.1% of N_f), and the length of the stage I crack is approximately 100 μm which is obviously longer than that in DF-8. In addition, the branch cracks propagating along MN planes are also observed in specimens DF-7 and DF-8.

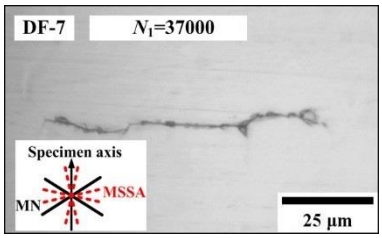

(a) Crack initiation in DF-7

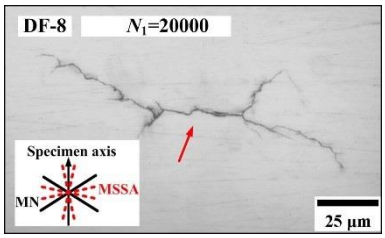

(b) Crack initiation in DF-8

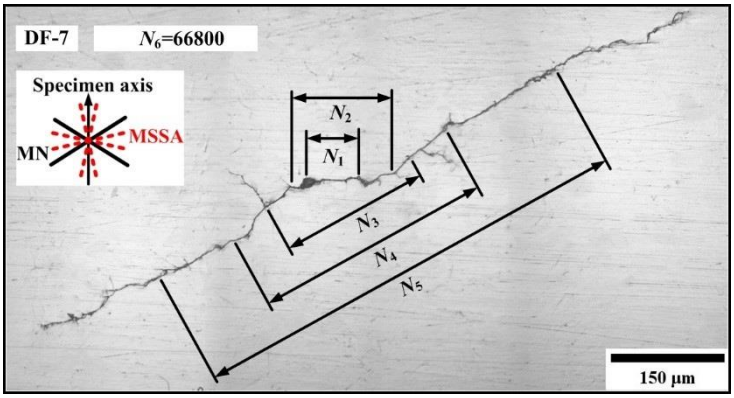

(c) Crack propagation in DF-7 (N_2 = 50,000, N_3 = 57,000, N_4 = 62,000, N_5 =65,000)

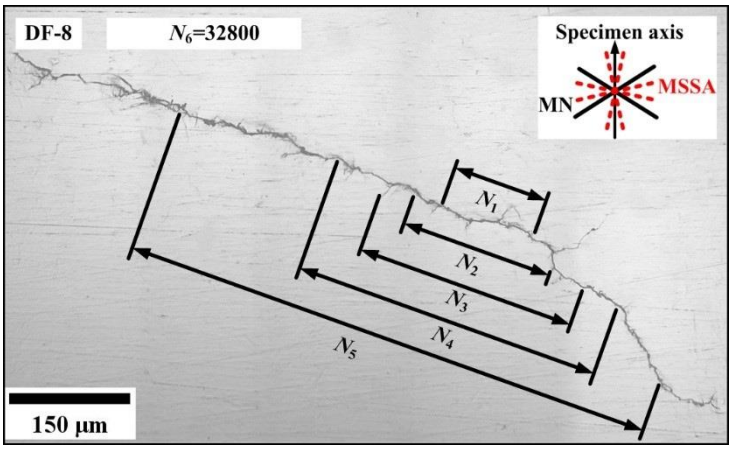

(d) Crack propagation in DF-8 (N_2 = 23,000, N_3 = 27,000, N_4 = 29,000, N_5 = 31,500)

Figure 11. Crack morphologies in specimens DF-7 and DF-8

Under AS-4, Figure 12 shows that several secondary cracks were observed in DF-7 at 66,800 blocks (95.0% of N_f) and in DF-8 at 32,800 blocks (92.2% of N_f). The directions of secondary crack initiation and propagation are almost consistent with those of the main cracks. Otherwise, the branch cracks are also observed, and propagate along the MN planes on specimen DF-8.

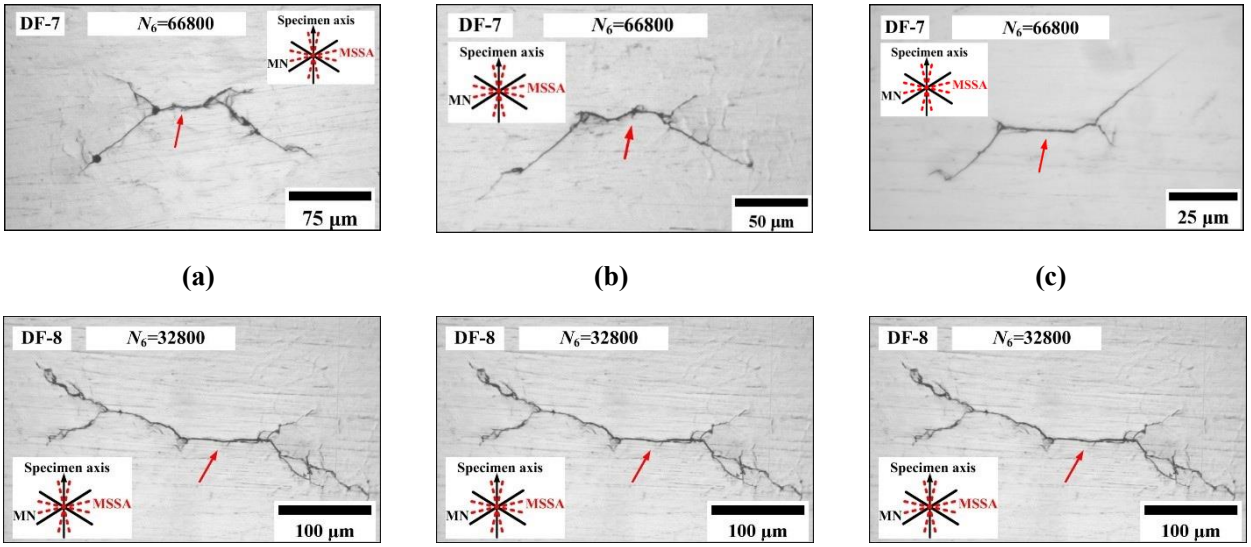

Figure 12. Secondary crack morphologies in specimens DF-7(a), (b), (c) and DF-8(d), (e), (f)

As discussed above, under multiaxial asynchronous fatigue loading with different frequency ratios, the surface crack initiates on the MSSA plane with a large normal stress and propagate along the MN planes. The number of secondary cracks increases as the tension or torsion frequency ratio increases. Under the same loading path, the morphologies of the main crack and secondary cracks are similar. For the condition where $\xi_1 = 2$ or $\xi_1 = 4$ and $\xi_2 = 1$, once the crack initiates, it will propagate rapidly.

3.4. Crack Length Versus Loading Blocks

The main surface crack lengths *versus* loading blocks of different specimens were recorded and are given in Table A1 and Figure 13. The test results from G-100 under constant amplitude loading path can be found in the authors' previous study[36]. The crack growth length Is significantly different between asynchronous loadings and constant amplitude loadings. However, the loading frequency has less of an effect on the crack growth lengths under different asynchronous loadings. The crack growth life of stage II accounts for more than 50% of N_f. When the crack length is approximately 500 μm, the crack propagation life accounts for more than 85% of N_f.

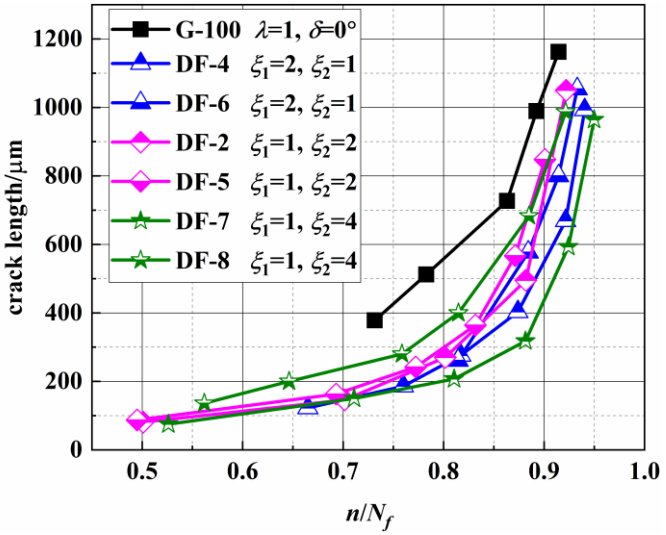

Figure 13. Crack length under different frequency ratios

4. Fatigue Life Prediction

4.1. Existing Multiaxial Cycle Counting Method

The counting process is more complex due to the coupling effect of tensile and shear stresses under multiaxial variable amplitude loading. Efforts have been made to apply the uniaxial cycle counting method to predict the multiaxial fatigue life. BS and WB methods are commonly used in dealing with multiaxial fatigue loadings[29, 30].

4.1.1. Bannantine and Socie Method

To identify multiaxial fatigue load reversals, Bannantine and Socie[18, 19] used the rainflow cycle counting method and critical plane criterion. Whether the tensile or shear critical plane damage parameter is chosen depends on the failure mode. When the shear stress is selected to count the cycle, the Fatemi-Socie[38] damage model (FS) is usually used and expressed as

$$\max_{\theta}\left\{\gamma_{na,\max}\left(1+k\frac{\sigma_{n,\max}}{\sigma_y}\right)\right\}=\frac{\tau_f'}{G}\left(2N_f\right)^{b_0}+\gamma_f'\left(2N_f\right)^{c_0} \tag{6}$$

When the tensile stress is selected for cycle counting, the Smith-Watson-Topper[35] damage model (SWT) is used and expressed as

$$\max_{\theta}\left\{\sigma_{n,\max}\cdot\varepsilon_{n,a}\right\}=\frac{\sigma_f'^2}{E}\left(2N_f\right)^{2b}+\sigma_f'\varepsilon_f'\left(2N_f\right)^{b+c} \tag{7}$$

An example of the BS with the SWT method to extract the reversal counting cycles under AS-2 is shown in Figure A1.

4.1.2. Wang and Brown Method

The WB method[20-22] was based on rainflow cycle counting and the von Mises equivalent strain/stress to identify all reversals. Then the damage can be calculated by the critical plane criterion or a modified strain-based multiaxial fatigue criterion due to Wang and Brown[39], as shown in Eq.(10), to obtain the total fatigue life. The Wang and Brown criterion can be expressed as

$$\frac{\gamma_{na,\max}+2S\varepsilon_{n,a}}{1+\nu'+\left(1-\nu'\right)S}=\frac{\sigma_f'-2\sigma_{n,m}}{E}\left(2N_f\right)^{b}+\varepsilon_f'\left(2N_f\right)^{c} \tag{8}$$

where S = 1.5-2.0 for steel materials.

An example of using the WB method to extract the reversal counting cycles under AS-2 is given in Figure A2.

4.2. Results and Discussion

The authors proposed a section critical plane method (SCPM)[40] for multiaxial high-cycle fatigue life prediction. Here it is also used for fatigue life prediction under asynchronous loadings.

To estimate the fatigue life under asynchronous loadings, the BS and WB cycle counting methods are used. Then, the fatigue life under simple cycles is predicted by the FS, SWT, WB and SPCM criteria. Finally, the fatigue life is got by the Palmgren-Miner's linear cumulative damage rule. The correlation between the experimental and prediction results of 30CrMnSiA steel under multiaxial asynchronous loadings is given in Figure 14. For multiaxial fatigue under stress loadings, there is no obvious engineering plastic strain. Hence only the elastic part is considered when the SWT, FS and WB criteria are used for fatigue life prediction.

Regarding the BS with the FS method, the prediction results lie outside of the 3 times range under AS-1, and others fall into the ±2 times range. The prediction results pertaining to BS with the SWT method are conservative and mostly exceed the 3 times range, and the discrepancies between the

experimental and prediction results are large. The prediction results obtained using the BS with the SCPM method all fall into the ±2 times range. Figure 14(d) and (e) show the results for S = 1.5 and S = 2.0, respectively, when calculating the WB damage parameter. When S = 1.5, the prediction life is nonconservative and lies in the -3 times fatigue life scatter band except for AS-2. When S = 2.0, the predicted fatigue life all lie in the ±3 times range, and they are nonconservative for the condition of AS-2, while the others are conservative. Regarding the WB with the SCPM method, the prediction results lie in the ±3 times range except the condition of AS-3.

Therefore, compared with other methods, the BS with the SCPM method is more appliable for 30CrMnSiA steel under asynchronous loadings.

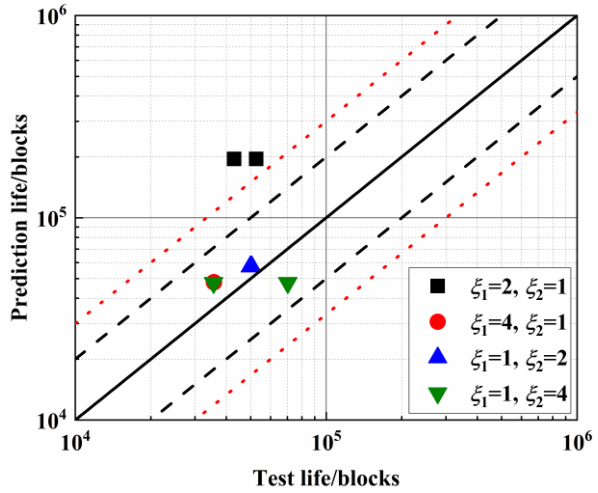

(a) BS with FS

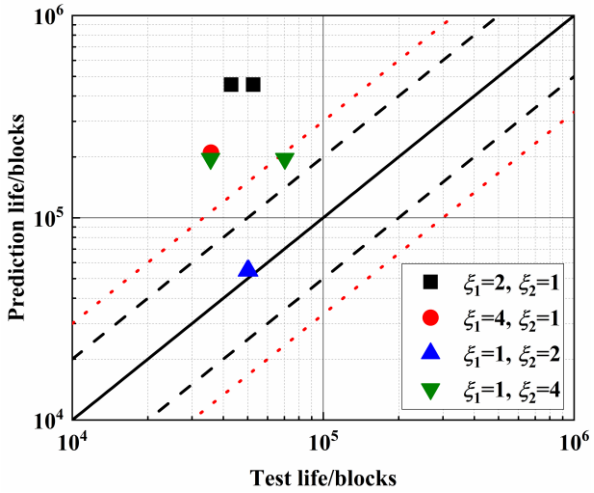

(b) BS with SWT

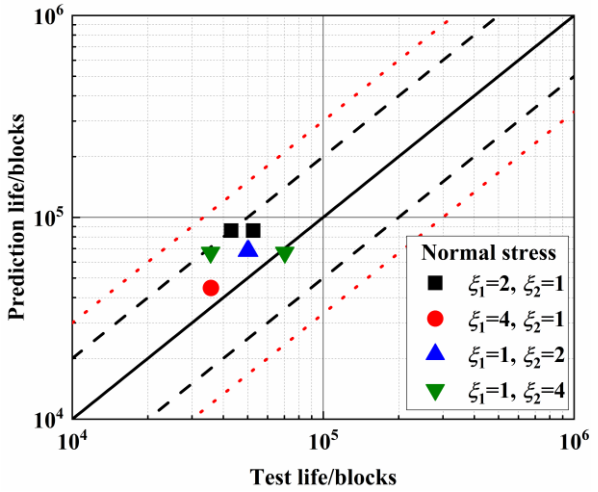

(c) BS with SCPM

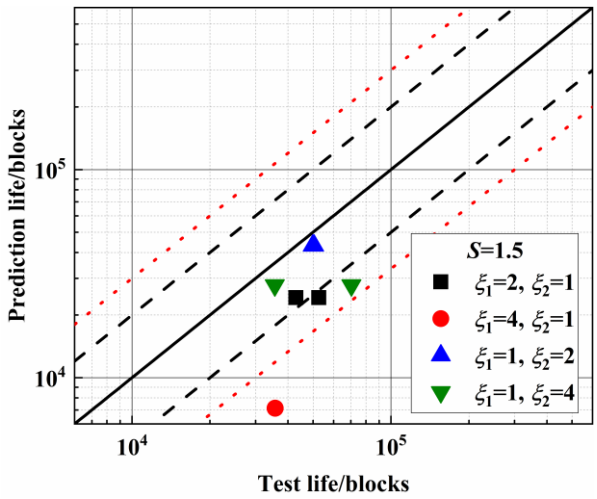

(d) WB with S=1.5

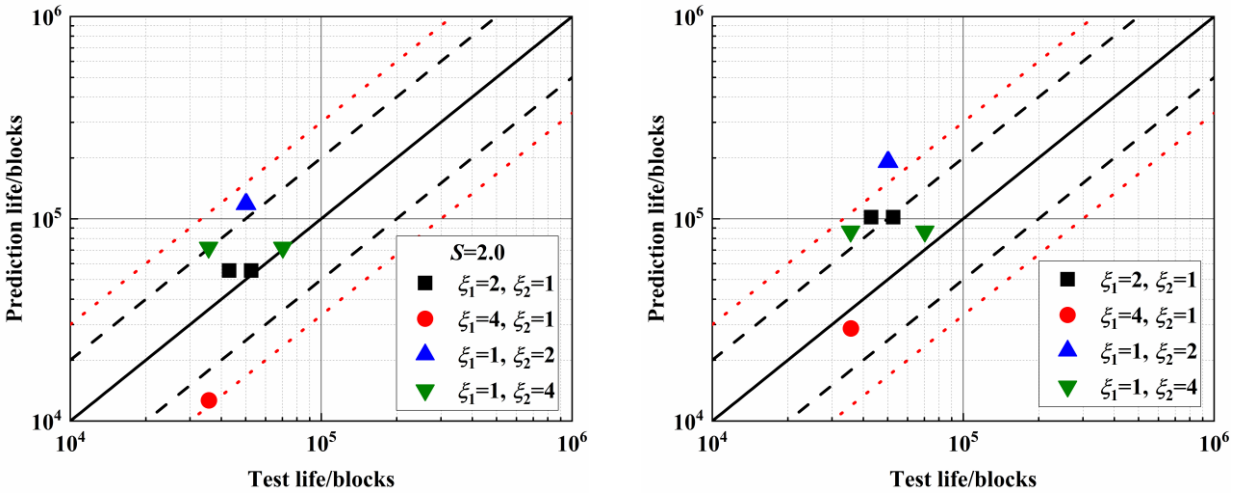

(e) WB with S = 2.0 **(f) WB with SCPM**

Figure 14. Prediction life *vs* test life under different frequency ratios

5. Conclusions

In this paper, multiaxial fatigue tests were performed on 30CrMnSiA steel under four asynchronous loadings. Subsequently, the effect of the frequency ratio on the fatigue failure life and crack behaviors were studied. As discussed above, the following conclusions can be drawn:

(a) The experimental results show that fatigue failure life under asynchronous loadings decreases when the value of ξ_1 or ξ_2 increases from 1 to 2, and there is no significant change when the value of ξ_1 or ξ_2 increases from 2 to 4.

(b) Based on the observation of the surface crack path, the crack initiates on the maximum shear stress amplitude plane and propagates along the maximum normal stress planes. A few secondary cracks propagating along the maximum normal stress planes were also observed. The number of secondary cracks increases as the value of ξ_1 or ξ_2 increases. Under asynchronous loadings, the frequency ratio has little effect on crack growth lengths. The proportion of the stage II crack propagation life is more than 50% of the fatigue failure life.

(c) The fatigue life was predicted by Bannantine-Socie and Wang-Browntwo cycle counting models with different criteria. The results indicate that the accuracy of the Bannantine-Socie model with the section critical plane method is higher than that of the others.

Nomenclature

E	Young's modulus
G	shear modulus
N_f	fatigue failure life

S	material parameter of Smith-Watson-Topper model
k	material parameter of Fatemi-Socie model
b	axial fatigue strength exponent
b_0	shear fatigue strength exponent
c	axial fatigue ductility exponent
c_0	shear fatigue ductility exponent
ξ_1	axial stress frequency
ξ_2	shear stress frequency
φ	direction of an arbitrary plane
ν'	effective Poisson Ratio
σ_y	tensile yield strength
σ_u	tensile ultimate strength
τ_y	torsional yield strength
τ_u	torsional ultimate strength
$\sigma_x(t)$	axial stress
$\sigma_{x,a}$	axial stress amplitude
$\tau_{xy}(t)$	shear stress
$\tau_{xy,a}$	torsion stress amplitude
$\sigma_n(t)$	cyclic normal stress on the plane of φ
$\tau_n(t)$	cyclic shear stress on the plane of φ
$\sigma_{n,max}$	maximum normal stress
$\sigma_{n,a}$	normal stress amplitude on the plane of φ
$\tau_{n,a}$	shear stress amplitude on the plane of φ
$\sigma_{n,m}$	mean normal stress
$\tau_{na,\max}$	maximum shear stress amplitude
$\gamma_{na,\max}$	maximum shear strain amplitude
$\varepsilon_{n,a}$	principal strain amplitude
σ'_f	axial fatigue strength coefficient
τ'_f	shear fatigue strength coefficient
ε'_f	axial fatigue ductility coefficient

γ'_f shear fatigue ductility coefficient

Abbreviations

AS asynchronous loading path

MN maximum normal

MSSA maximum shear stress amplitude

Acknowledgements

The authors thank the Geological Laboratory of Chongqing University.

Funding information

National Nature Science Foundation of China: 11702012, 11772028, 11872131, U1864208 and 11572058

Conflict of interest

The authors declare that there is no conflict of interest that could be perceived as prejudicing the impartiality of the research reported.

Author Contribution

Funding acquisition, Jianyu Zhang; Investigation, Xinhong Shi; Writing – original draft, Tianqi Liu and Xinxin Qi; Writing – review & editing, Limin Gao and Tian Zhang.

Data Availability Statement

Data are available on request to the authors

Appendix

Table A1 Crack lengths *versus* loading blocks of different specimens

Spec. ID	Contents	N_1	N_2	N_3	N_4	N_5	N_6
DF-4	blocks	35000	40000	43000	46000	48500	49500
	$2a$/μm	122.5	186	276	403	669	993
DF-6	blocks	35000	38000	39300	40100	--	--
	$2a$/μm	261	577	800	1054		
DF-2	blocks	25000	35000	40000	44000	46000	--
	$2a$/μm	81	146	270	495	1050	
DF-5	blocks	25000	35000	39000	42000	44000	45500
	$2a$/μm	87	163	242	364	567	848
DF-9	blocks	32000	--	--	--	--	--
	$2a$/μm	920	--	--	--	--	--
DF-7	blocks	37000	50000	57000	62000	65000	66800
	$2a$/μm	75	150	207	318	593	964
DF-8	blocks	20000	23000	27000	29000	31500	32800
	$2a$/μm	136	200	280	400	683	987

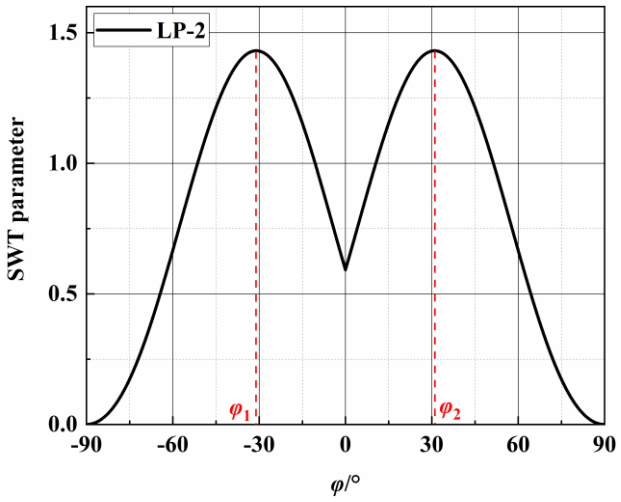

(a) SWT parameter

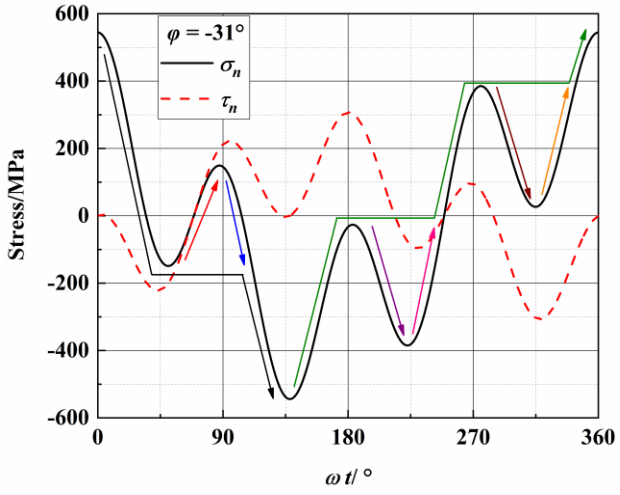

(b) φ = - 31°

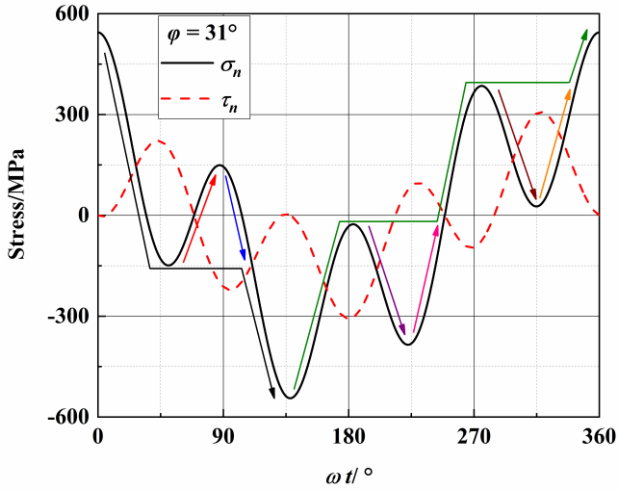

(c) φ = 31°

Figure A1. The procedure and results of BS with SWT method for reversal extraction under LP-2

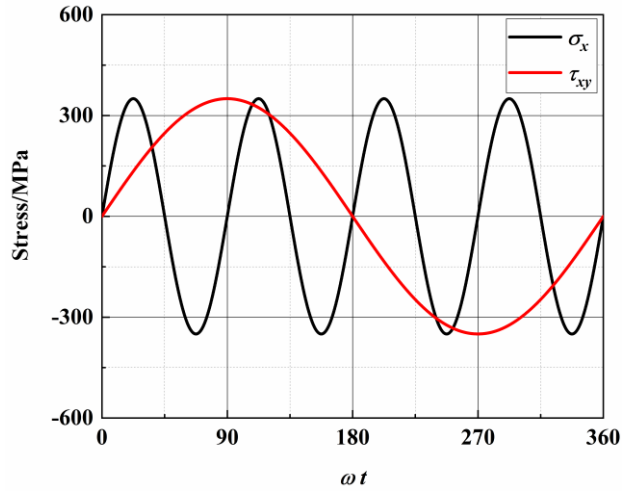

(a) variation of stress in a loading block

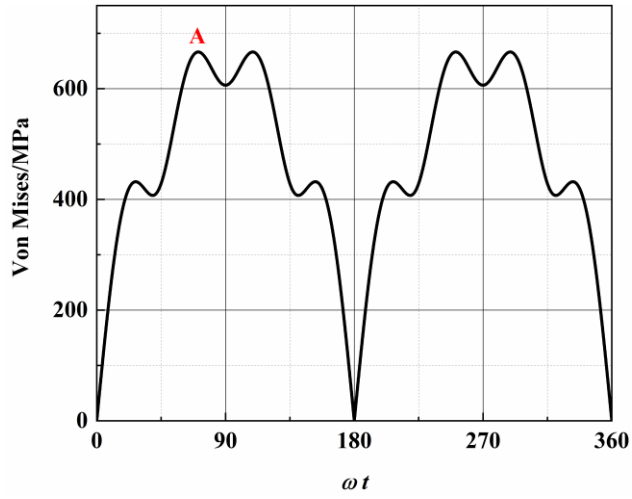

(b) von Mises

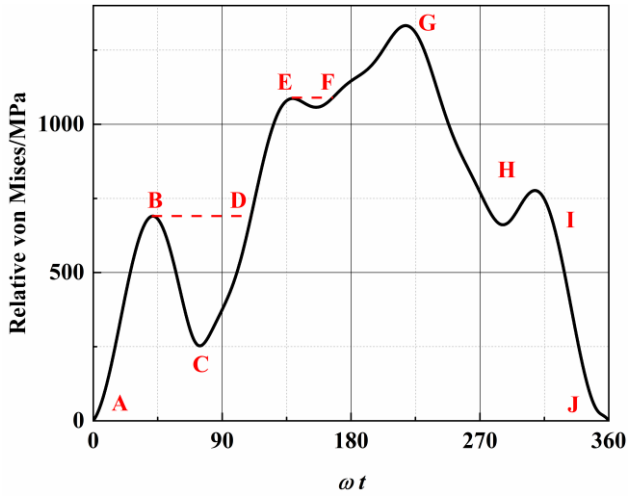

(c) 1st reversal (A-B-D-E-F-G)

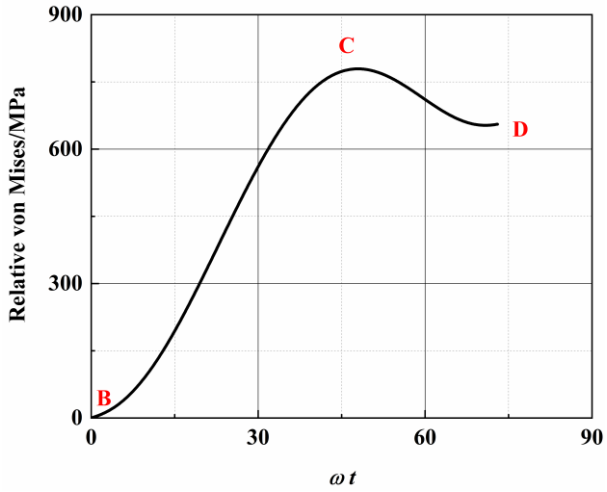

(d) 2nd reversal (B-C)

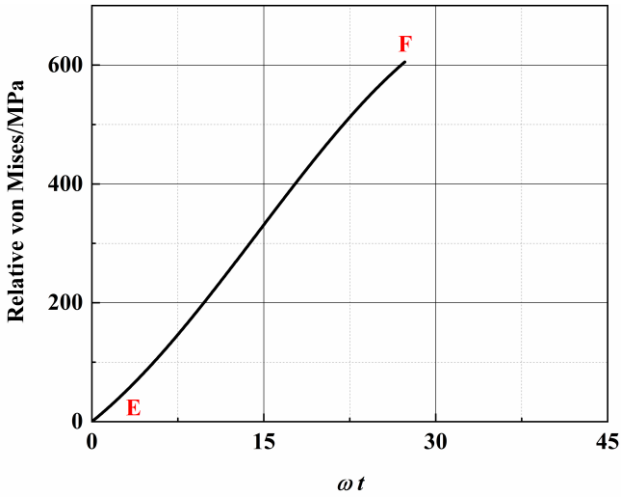

(e) 3rd reversal (E-F)

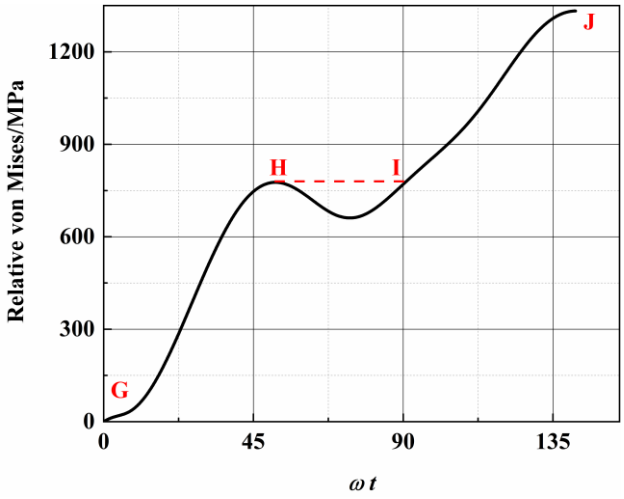

(f) 4th reversal (G-H-I-J)

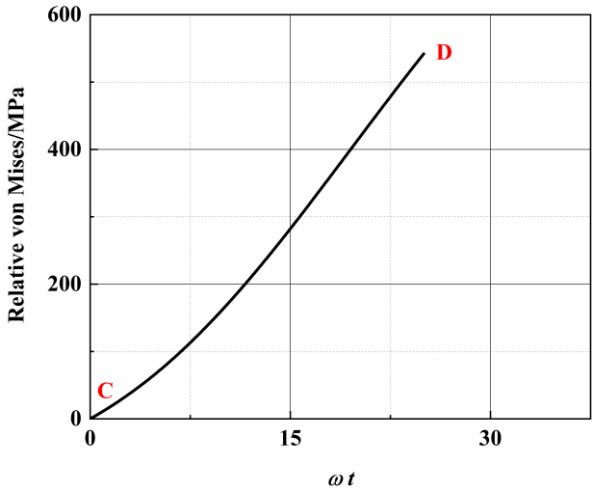

(g) 5th reversal (C-D)

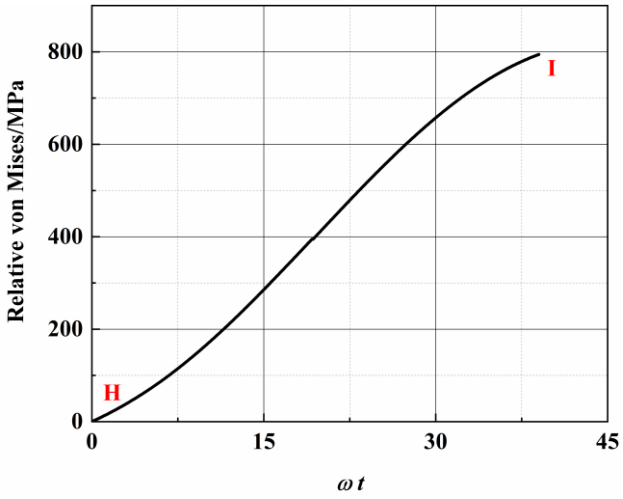

(h) 6th reversal (H-I)

Figure A2. The procedure and results of WB method for reversal extraction under LP-2

References

1. Mei, J.; Dong, P., Modeling of path-dependent multi-axial fatigue damage in aluminum alloys. *International Journal of Fatigue* **2017,** *95*, 252-263.
2. Mei, J.; Dong, P., An equivalent stress parameter for multi-axial fatigue evaluation of welded components including non-proportional loading effects. *International Journal of Fatigue* **2017,** *101*, 297-311.
3. Mei, J.; Dong, P., A new path-dependent fatigue damage model for non-proportional multi-axial loading. *International Journal of Fatigue* **2016,** *90*, 210-221.
4. Jiang, Y.; Hertel, O.; Vormwald, M., An experimental evaluation of three critical plane multiaxial fatigue criteria. *International Journal of Fatigue* **2007,** *29* (8), 1490-1502.
5. Hoffmeyer, J.; Doring, R.; Seeger, T.; Vormwald, M., Deformation behaviour, short crack growth and fatigue livesunder multiaxial nonproportional loading. *International Journal of Fatigue* **2006,** *28* (5-6), 508-520.
6. Noban, M.; Jahed, H.; Winkler, S.; Ince, A., Fatigue characterization and modeling of 30CrNiMo8HH under multiaxial loading. *Materials Science and Engineering: A* **2011,** *528* (6), 2484-2494.
7. Mielke, S. Untersuchungen zum festigkeitsverhalten bei mehrachsiger randombeanspruchung unter biegung und torsion. Technische Universitat Clausthal, Clausthal Zellerfeld, 1980.
8. McDiarmid, D. L., Fatigue under out-of-phase biaxial stresses of different frequencies. *ASTM Spec Tech Publ* **1985**, 606-621.
9. Mcdiarmid, D. L., Mean stress effects in biaxial fatigue where the stresses are out-of-phase and at different frequencies. *Biaxial/Multiaxial Fatigue* **1989,** *53*, 1-18.
10. McDiarmid, D. L., The effect of mean stress on biaxial fatigue where the stresses are out-of-phase and at different frequencies. *Biaxial/Multiaxial Fatigue* **1989**, 605-619.
11. Heidenreich, R.; Richter, I.; Zenner, H., Schubspannungsintensittshypothese - weitere experimentelle und theoretische untersuchungen. *Konstruktion* **1984,** *36*, 99-104.
12. Bernasconi, A.; Foletti, S.; Papadopoulos, I., A study on combined torsion and axial load fatigue limit tests with stresses of different frequencies. *International Journal of Fatigue* **2008,** *30* (8), 1430-1440.
13. Reis, L.; Li, B.; De Freitas, M., Multiaxial loadings with different frequencies between axial

and torsional components in 42CrMo4 steel. *International Journal of Structural Integrity* **2010,** *1* (4), 303-313.

14. Pejkowski, Ł.; Skibicki, D., Stress-strain response and fatigue life of four metallic materials under asynchronous loadings: Experimental observations. *International Journal of Fatigue* **2019,** *128*, 105202.
15. Pejkowski, Ł.; Seyda, J., Fatigue of four metallic materials under asynchronous loadings: Small cracks observation and fatigue life prediction. *International Journal of Fatigue* **2021,** *142*, 105904.
16. Endo, T.; Mitsunaga, K.; Takahashi, K.; Kobayashi, K.; Matsuishi, M., Damage evaluation of metals for random or varying loading-three aspects of rain flow method. *Mechanical Behavior of Materials* **1974**, 371-380.
17. Varvani-Farahani, A., Critical plane-energy based approach for assessment of biaxial fatigue damage where the stress-time axes are at different frequencies. *European Structural Integrity Society* **2003,** *31*, 203-221.
18. Bannantine, J.; Socie, D., A variable amplitude multiaxial fatigue life prediction method. *Biaxial/Multiaxial Fatigue* **1989**, 35-51.
19. Bannantine, J.; Socie, D., A multiaxial fatigue life estimation technique. *ASTM Special Technical Publication* **1992**, 245-275.
20. Wang, C. H.; Brown, M. W., On plastic deformation and fatigue under multiaxial loading. *Nuclear Engineering and Design* **1996,** *162* (1), 75-84.
21. Wang, C. H.; Brown, M. W., Life prediction techniques for variable amplitude multiaxial fatigue--part 2: Comparison with. *Journal of Engineering Materials & Technology* **1996,** *118* (3), 371.
22. Wang, C. H.; Brown, M. W., Life prediction techniques for variable amplitude multiaxial fatigue--part 1: Theories. *Journal of Engineering Materials & Technology* **1996,** *118* (3), 367.
23. Meggiolaro, M. A.; De Castro, J. T. P., An improved multiaxial rainflow algorithm for non-proportional stress or strain histories – Part II: The Modified Wang–Brown method. *International Journal of Fatigue* **2012,** *42*, 194-206.
24. Meggiolaro, M. A.; De Castro, J. T. P., An improved multiaxial rainflow algorithm for non-proportional stress or strain histories – Part I: Enclosing surface methods. *International Journal*

of Fatigue **2012,** *42*, 217-226.

25. Wei, Z.; Dong, P., A rapid path-length searching procedure for multi-axial fatigue cycle counting. *Fatigue & Fracture of Engineering Materials & Structures* **2012,** *35* (6), 556-571.
26. Dong, P.; Wei, Z.; Hong, J. K., A path-dependent cycle counting method for variable-amplitude multi-axial loading. *International Journal of Fatigue* **2010,** *32* (4), 720-734.
27. Wei, Z.; Dong, P., Multiaxial fatigue life assessment of welded structures. *Engineering Fracture Mechanics* **2010,** *77* (15), 3011-3021.
28. Shang, D.; Wang, D.; Xu, H.; Ping, A., A unified multiaxial fatigue damage parameter. *Acta Mechanica Solida Sinica* **1998,** *11* (3), 261-274.
29. Anes, V.; Reis, L.; Li, B.; De Freitas, M., New cycle counting method for multiaxial fatigue. *International Journal of Fatigue* **2014,** *67*, 78-94.
30. Anes, V.; Reis, L.; Freitas, M., Asynchronous multiaxial fatigue damage evaluation. *Procedia Engineering* **2015,** *101*, 421-429.
31. Anes, V.; Reis, L.; Li, B.; Fonte, M.; De Freitas, M., New approach for analysis of complex multiaxial loading paths. *International Journal of Fatigue* **2014,** *62*, 21-33.
32. Lee, B., Fatigue analysis under variable amplitude loading using an energy parameter. *International Journal of Fatigue* **2003,** *25* (7), 621-631.
33. Janssens, K. G. F., Universal cycle counting for non-proportional and random fatigue loading. *International Journal of Fatigue* **2020,** *133*, 105409.
34. Arora, P.; Gupta, S. K.; Samal, M. K.; Chattopadhyay, J., Multiaxial fatigue tests under variable strain paths and asynchronous loading and assessment of fatigue life using critical plane models. *International Journal of Fatigue* **2021,** *145*, 106049.
35. Smith, K. N.; Watson, P.; Topper, T. H., Stress- strain function for the fatigue of metals. *J Mater* **1970**.
36. Liu, T.; Shi, X.; Zhang, J.; Fei, B., Crack initiation and propagation of 30CrMnSiA steel under uniaxial and multiaxial cyclic loading. *International Journal of Fatigue* **2019,** *122*, 240-255.
37. Murakami, Y., *Metal fatigue: effects of small defects and nonmetallic inclusion*. Academic Press & Elsevier: London, 2019.
38. Fatemi, A.; Socie, D. F., A critical plane approach to multiaxial fatigue damage including out-

of-phase loading. *Fatigue & Fracture of Engineering Materials and Structures* **1988,** *11* (3), 149-165.

39. Wang, C. H.; Brown, M. W., A path-independent parameter for fatigue under proportional and non-proportional loading. *Fatigue & Fracture of Engineering Materials and Structures* **1993,** *16* (12), 1285-1297.

40. Qi, X.; Liu, T.; Shi, X.; Wang, J.; Zhang, J.; Fei, B., A sectional critical plane model for multiaxial high-cycle fatigue life prediction. *Fatigue & Fracture of Engineering Materials & Structures* **2021,** *44* (3), 689-704.